RESEARCH Revista Mexicana de Física **61** (2015) 400–413 NOVEMBER-DECEMBER 2015

Time evolution of spinor perturbations in regular black holes

O. Pavel Fernández Piedra, J. Bernal Castillo, F. Sosa Nuñez and Y. Jiménez Santana
Grupo de Estudios Avanzados, Universidad de Cienfuegos,
Carretera a Rodas, Cuatro Caminos, s/n. Cienfuegos, Cuba.
e-mail: opavel@ucf.edu.cu; jbernal@ucf.edu.cu; fsosa@ucf.edu.cu; yjsantana@ucf.edu.cu

Received 17 March 2015; accepted 29 June 2015

In this report we present results concerning the study of complete time evolution of massless fermion perturbations propagating in several four dimensional regular black hole space-times. The black hole solution arises from coupling gravity with external matter sources, like non-linear electrodynamics or some phantom fields. After numerical integration we obtain the time evolution profiles for fermion fields in this space-times. By fitting the numerical data, we compute the quasinormal frequencies that characterize the test field evolution at intermediary times, and for late times, we find power law tails, in strong similarity with usual results for non regular black holes. Quasinormal modes was also investigated using a WKB approach at six order beyond the eikonal limit, obtaining a good correspondence with the numerical calculated frequencies.

Keywords: Regular black hole; spinor perturbations; Dirac fields.

PACS: 02.30Gp; 03.65ge

1. Introduction

The study of perturbations around black hole solutions can be traced back to the work of Regge and Wheeler in 1957 [1]. It is well known that the time evolution of such perturbations outside the horizon can be divided in three stages. Firstly we have an initial wave burst that comes directly from the source of perturbation and consequently is strongly dependent on the initial wave form of the fluctuation. Following this initial transient stage, the system undergo proper damped quasinormal oscillations, whose frequencies and damping rates are completely fixed by the geometric structure of the black hole spacetime, and the physical properties of the test perturbation. Finally, that quasinormal ringing is followed by tails at late times, whose exponent are different for each multipole number describing the mode, and, for higher dimensional spacetimes, depends on the dimensionality of the background. Power law tails are typical for asymptotically flat spacetimes, whereas for asymptotically de Sitter backgrounds we can observe also exponential tails. The situation is different for AdS black holes, in which the complete time evolution is dominate by quasinormal oscillations [2-5].

As quasinormal frequencies encode information on the black hole space-time geometry, it is possible, for example, estimate the charge, mass and angular momentum of the black hole from it [4,5]. Quasinormal frequencies also depends on the parameters that characterize the perturbing fields. Thus, the propagations of disturbances of different spin weight is an important subject to study in such backgrounds.

As fermions universally describe some matter fields, in most cases they are essential for the structure of the solutions, raising the importance to study fermion fluctuations. Fermions perturbations has been studied for four dimensional black holes solution, but also in higher dimensional black holes backgrounds [7-12].

On other hand, the avoidance of singularities in Gravity theories is an old problem. In 1968 Bardeen proposed the first model of a regular black hole without singularity, that satisfied the weak energy condition [13]. This regular black hole was interpreted as a solution describing the gravitational field of a magnetic monopole in nonlinear electrodynamics [13]. After Bardeen's model, several regular black hole solution has been proposed in different contexts [15-20]. All this black hole solution arises from coupling gravity with external matter sources, like non-linear electrodynamics or some phantom fields.

Concerning perturbations in the above mentioned black hole backgrounds, in a previous paper Flachi and Lemos determined the quasinormal modes of scalar perturbations [21] and Li, Ma and Lin studied a Dirac field [22]. In those papers the authors perform the calculations using mainly a WKB approximation developed by Iyer and Will [23]. However, they only studied quasinormal modes, and not the complete time evolution of perturbations.

This paper is devoted to the study the complete evolution of massless fermion fluctuations in all the above mentioned regular black holes backgrounds [13,15-20]. Not only the quasinormal ringing is sudied, but also late time tails that it is expected to appear in those gravitational backgrounds. The paper is organized as follows: Section 2 briefly presents the regular black holes considered in the rest of this work. In Sec. 3 we present the evolution equations for fermion fields in spherically symmetric space-times, and Sec. 4 is devoted to describe the numerical solution of the evolution equations for regular black hole backgrounds. In Sec. 5 we present the results for quasinormal frequencies, and in Sec. 6 we analyze the late time tails present in the dynamic evolution of the fermion fluctuations. Finally, we present our conclusions.

2. Regular black hole Solutions

The space-times of all the regular black hole solutions [13,15-20] considered in this paper can be described by the line element

$$ds^2 = -f(r)dt^2 + f^{-1}(r)dr^2 + r^2 d\Omega_2^2(\theta,\phi). \quad (1)$$

where $d\Omega_2^2 = d\theta^2 + \sin^2\theta d\phi^2$ describes the unit two-sphere.

In the rest of this section we closely follow the brief review in Sec. 2 of Ref. 21, adding some minor information from the original references. Regular black hole solutions can be founded by coupling gravity with a properly matter source through a typical action defined as:

$$S = \frac{1}{16\pi}\int d^4x\sqrt{-g}\,(R - \mathscr{L}) \quad (2)$$

where g is determinant of the metric tensor, R is the Ricci scalar, and $\mathscr{L}$ represents the Lagrangian density of the matter source.

The first solution that will be consider in this paper was proposed by Bardeen in Ref. 13, and reinterpreted in Ref. 14 as a magnetic solution to Einstein equations coupled to nonlinear electrodynamics with matter Lagrangian density given by

$$\mathscr{L}(F) = \frac{3}{2s\alpha^2}\left(\frac{\sqrt{2\,\alpha^2 F}}{1+\sqrt{2\,\alpha^2 F}}\right)^{5/2},$$

with $F \equiv (1/4)F_{\mu\nu}F^{\mu\nu}$, being $F^{\mu\nu}$ the electromagnetic field strength. In this model the parameter α can be interpreted as the charge of the self-gravitating magnetic monopole [14], and its numerical value, as well as those of the mass m, determine if the solution have zero, one or two horizons. The line element of Bardeen's regular black hole is given by (1) with:

$$f(r) = 1 - \frac{2mr^2}{(r^2+\alpha^2)^{3/2}}. \quad (3)$$

A quite similar solution was founded by Hayward in Ref. 15, in which:

$$f(r) = 1 - \frac{2mr^2}{r^3+2l^2m} = 1 - \frac{2mr^2}{r^3+2\alpha^2}. \quad (4)$$

As pointed out in Ref. 21, this solution requires a matter source whose energy-momentum tensor is de-Sitter at the core and vanishes at spatial infinity. The parameter α is related with the de Sitter core radius L and the mass m through $\alpha = L\sqrt{m}$. For this solution the existence and number of horizons is again determined by the relative values of m and L (or α). As we can easily observe, in the limit $\alpha \to 0$ the Bardeen and Hayward solutions reduce to the Schwarzschild black hole.

Another magnetically charged solution is given by Bronnikov in Ref. 16, where he used $\mathscr{L}(F) = F/\cosh^2\left(a|F/2|^{1/4}\right)$ to obtain the line element (1) with

$$f(r) = 1 - \frac{2m}{r}\left(1 - \tanh\frac{r_0}{r}\right). \quad (5)$$

The above result, (5), was also obtained in Ref. 17, as the zeroth order perturbative solution of the equations of motion coming from quadratic gravity coupled with nonlinear electrodynamics, using for the matter source the lagrangian density

$$\mathscr{L}(F) = F\left[1 - \tanh^2\left(s\sqrt[4]{\frac{Q^2F}{2}}\right)\right],$$

where $s = |Q|/2b$, Q is the magnetic charge of the solution and b is a free parameter. In this model, s and b can be adjusted for obtain regularity at the center [17]. Schwarzschild black hole is obtained from the above solution in the limit $r_0 \to 0$.

Nonlinear electrically charged configurations can lead to regular black holes solutions. In Ref. 19, Ayón-Beato and García proposed a model in which

$$f(r) = 1 - \frac{2mr^2}{(r^2+q^2)^{3/2}} + \frac{q^2r^2}{(r^2+q^2)^2} \quad (6)$$

In the above solution m and q are respectively the mass and the electric charge of the configuration. For charges below some critical value q_c, we have a solution with separated inner and event horizon, respectively. For $q = q_c$ the horizons shrink into a single one leading to an extreme black hole solution, whereas for $q > q_c$ the horizon structure are absent, and we are in presence of a globally regular gravitational background.

It is important to mention that solution (6), as discussed in Ref. 16 by Bronnikov, should be taken with care, due to the presence of some cusps in the Lagrangian density, which implies that the regular electric solution correspond to different Lagrangians in different parts of space. However, as in Ref. 21, taking into account that the above solution coincides with a Schwarzschild black hole for $q = 0$, we will take this as a good example for check the validity of our calculational schemes.

Using the results of Ref. 16 on the basic properties that the Lagrangian density $\mathscr{L}(F)$ can have, for lead to an electrically charged regular black hole configuration, Dymnikova shows in Ref. 18 that, for certain non-linear electrodynamics sources, there exist solutions with

$$f(r) = 1 - \frac{4m}{\pi r}\left(\tan^{-1}\frac{r}{r_0} - \frac{rr_0}{r^2+r_0^2}\right). \quad (7)$$

which satisfies the weak energy condition. In the above expression $r_0 = \pi q^2/(8m)$ is a length scale parameter involving the mass m and the charge q of the electric solution. In the limit $r_0 \to 0$, the solution coincides with the Schwarzschild black hole.

The last gravitational background to be considered in this paper is presented in Ref. 20. It comes from coupling gravity with a phantom field, using an action of the form

$$S = \int \sqrt{g}\, d^4x[R + \varepsilon g^{\mu\nu}\partial_\mu\phi\partial_\nu\phi - 2V(\phi)] \quad (8)$$

where ε is set to -1. The solution obtained is given by (1) with

$$f(r)=1+\frac{cr^2}{b^2}+\frac{\rho_0 r^2}{b^3}\left(\frac{b\sqrt{r^2-b^2}}{r^2}+\tan^{-1}\frac{\sqrt{r^2-b^2}}{b}\right) \quad (9)$$

The parameters b, c and ρ_0 characterize the features of the phantom potential field $U(b,c,\rho_0)$. In this paper, we fix the values of c and ρ_0 as $c=-(3\pi/2b)$ and $\rho_0=3$, corresponding to a black hole with unit mass. As in the other regular black hole solutions, we can obtain the Schwarzschild black hole in the limit $b\to 0$.

3. Massless Dirac perturbations

In curved space-time the massless Dirac equation is:

$$\nabla\!\!\!/\psi=\Gamma^\mu\nabla_\mu\psi=0 \quad (10)$$

where $\nabla\!\!\!/$ is the Dirac Operator, Γ^μ are the gamma matrices of the curved space-time, the covariant derivative is defined as $\nabla_\mu=\partial_\mu-(1/4)w_\mu^{ab}\gamma_a\gamma_b$, with μ and a being the tangent and space-time indices respectively, related by the basis of one forms $\vec{e}^{\,a}\equiv e^a_\mu$. The connection $\omega^{ab}_\mu\equiv\omega^{ab}$ obey the relation $d\vec{e}^{\,a}+\omega^a_b\wedge\vec{e}^{\,b}=0$, being γ_a the gamma matrices of flat space-time, related with the curved space-time ones trough $\Gamma^\mu=e^\mu_a\gamma^a$. It form a Clifford algebra and consequently satisfy the anti-commutation relations $\{\gamma^a,\gamma^b\}=-2\eta^{ab}$ con $\eta^{00}=-1$.

In Refs. 7, 9, 24 is its showed that by writing $\psi=r^{-3}\sum_\ell\left(\tilde{\varphi}^{(+)}_\ell\tilde{\xi}^{(+)}_\ell+\tilde{\varphi}^{(-)}_\ell\tilde{\xi}^{(-)}_\ell\right)$ where

$$\tilde{\varphi}^{(+)}_\ell=\begin{pmatrix} i\zeta_\ell(t,r)\\ \chi_\ell(t,r)\end{pmatrix}, \quad (11)$$

the Dirac equation in the general spherically symmetric background can be put as a simple pair of evolution equations, one for each component of the spinor $\tilde{\varphi}$:

$$\frac{\partial^2\zeta_\ell}{\partial t^2}-\frac{\partial^2\zeta_\ell}{\partial r_*^2}+V_+(r)\zeta_\ell=0, \quad (12)$$

$$\frac{\partial^2\chi_\ell}{\partial t^2}-\frac{\partial^2\chi_\ell}{\partial r_*^2}+V_-(r)\chi_\ell=0, \quad (13)$$

where:

$$V_\pm=\pm\frac{d\Lambda_\ell}{dr_*}+\Lambda_\ell^2 \quad (14)$$

and the function $\Lambda_\ell(r)$ is given by

$$\Lambda_\ell(r)=\frac{\sqrt{f(r)}}{r}\left(\ell+1\right). \quad (15)$$

The above equations gives the temporal evolution of Dirac perturbations outside the black hole spacetime. $\zeta_\ell(t,r)$ and $\chi_\ell(t,r)$ will have similar time evolutions and then they will have the same spectra, both for scattering and quasinormal, due to the supersymmetric character of the potentials V_+ and V_- [25]. In the following we will work with Eq. (12)

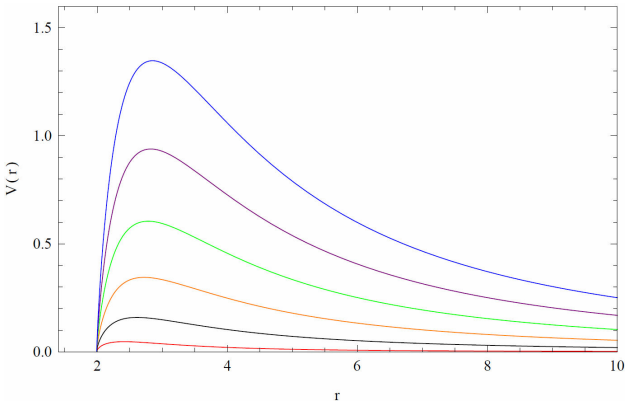

FIGURE 1. Potential for Dirac perturbations with $\ell=0$ (bottom) to $\ell=5$ (top) and $\alpha=0.1$ in Bardeen's regular black hole.

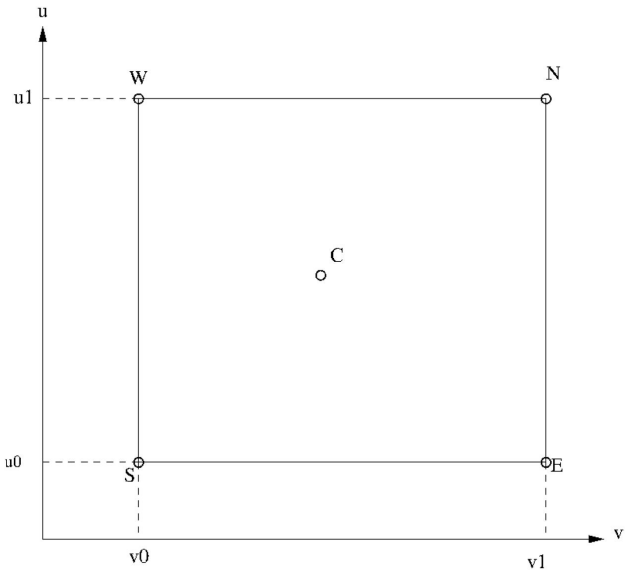

FIGURE 2. Integration grid in the plane (u,v) limited by the points N, S, E, W and C. This cell represents an integration step, and the initial data are specified on the left and bottom sides of the rhombus.

and we eliminate the subscript $(+)$ for the effective potential, defining $V(r)\equiv V_+(r)$.

In Fig. 1 we show effective potential profiles for massless Dirac perturbation in the four dimensional black hole background of Ref. 13. The profiles for other regular black holes are similar. In all cases, the potential has the form of a definite positive barrier. Then, we can expect at intermediary times well defined damped quasinormal oscillations in the evolution of fermion perturbations outside this spacetimes. This fact will be confirmed in the next sections.

4. Time evolution of Dirac perturbations

In order to solve the Eq. 12, we first developed a finite difference scheme (12). We discretize (12) taking $t=t_0+k\Delta t$ and $r_*=r_{*0}+j\Delta r_*$, and rewrite the equation as

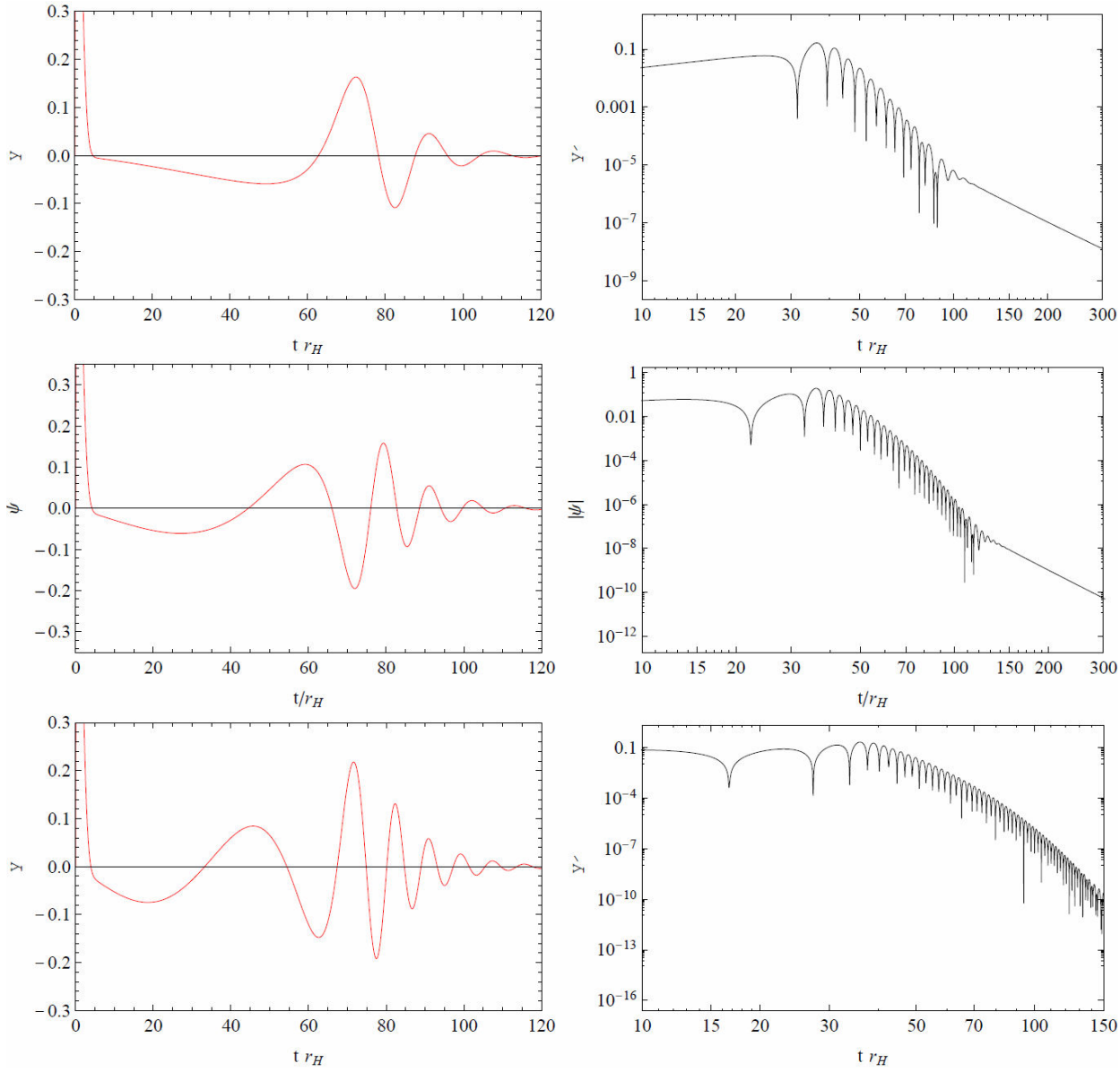

FIGURE 3. Normal (left) and logarithmic (right) plots of the time-domain evolution of massless Dirac perturbations in Bardeen's regular black holes with $\alpha = 0.1$. From top to bottom: $\ell = 1, 2, 3$.

$$\psi^j_{k+1} = -\psi^j_{k-1} + \frac{\Delta t^2}{\Delta r_*^2}\left(\psi^{j+1}_k + \psi^{j-1}_k\right) + \left(2 - 2\frac{\Delta t^2}{\Delta r_*^2} - V_j \Delta t^2\right)\psi^j_k, \tag{16}$$

We also chose as initial condition a static Gaussian distribution

$$\psi\left(r_*, t_0\right) = Ae^{-a(r_* - b)^2}, \qquad \frac{\partial}{\partial t}\psi\left(r_*, t\right)|_{t=t_0} = 0. \tag{17}$$

Applying the Von Neumann stability condition to the above difference equation results in the relation

$$\frac{\Delta t^2}{\Delta {r_*}^2}\sin^2\left(\frac{\alpha}{2}\right) + \frac{\Delta t^2}{4}V(\alpha) < 1$$

Then, defining $V_{\max}$ as the largest value of V_j in the numerical grid, our numerical solution will be stable if

$$\frac{\Delta t^2}{\Delta r_*^2} + \frac{\Delta t^2}{4}V_{\max} < 1 \tag{18}$$

We can now take $\Delta t = (1/2)\Delta r_*$ and choose a sufficiently small time step such that $V_{\max} < (3/\Delta t^2)$ for assure the stability of our numerical codes. In all the calculations we verified that this stability condition is fulfilled.

We also implemented the characteristic integration scheme developed by Gundlach, Price and Pullin [27] to check the numerical results.

As a first step, we introduced in (12) light-cone coordinates $du = dt - dr_*$ and $dv = dt + dr_*$ to obtain

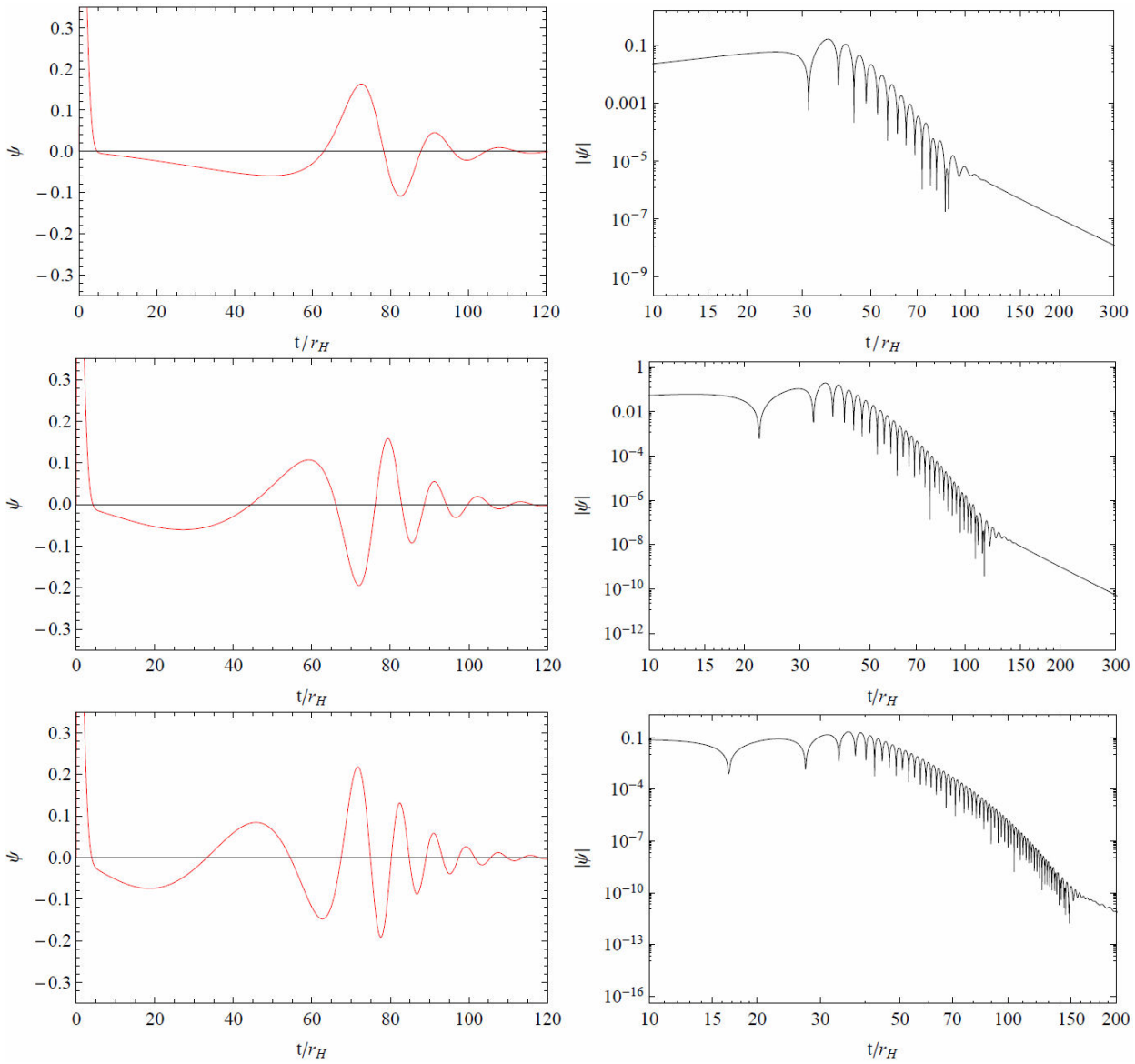

FIGURE 4. Normal (left) and logarithmic (right) plots of the time-domain evolution of massless Dirac perturbations in Hayward's regular black holes with $\alpha = 0.1$. From top to bottom: $\ell = 1, 2, 3$.

$$\left(4\frac{\partial^2}{\partial u \partial v} + V(u,v)\right)\zeta_\ell(u,v) = 0. \tag{19}$$

The next step is to discretize the above equation on a grid with a typical cell of a given integration step showed in Fig. 2, where the letters S, W, E, N are used to mark the points that limits this particular integration cell according to: $S = (u, v)$, $W = (u + \Delta u, v)$, $E = (u, v + \Delta v)$, $N = (u + \Delta u, v + \Delta v)$. The discretized version of (19) that we used was

$$\zeta_\ell(N) = \zeta_\ell(W) + \zeta_\ell(E) - \zeta_\ell(S) - \frac{\Delta u \Delta v}{8} V(S)\left(\zeta_\ell(W) + \zeta_\ell(E)\right) + \mathcal{O}(h^4), \tag{20}$$

We see that the field value at point N only depends on the field values at S, E and W. For a set of initial conditions at the two null surfaces $u = u_0$ and $v = v_0$, we can find, using (20), the value of the field ζ_ℓ inside the rhombus builded on this two null surfaces. Now iterating the integration cell, we can find the complete data that gives the evolution of the fields in time. Then fitting the numerical data at the corresponding region of the profile, it is possible to find the quasi-normal frequencies.

The Figs. 3-8 show the time domain profile of the evolution of Dirac massless perturbations in all the regular black hole solutions under study. As we can see, in all the regular black holes studied the Dirac perturbation follow the usual dynamics in time domain. First, we observe an initial transient stage, that is strongly dependent upon the initial shape

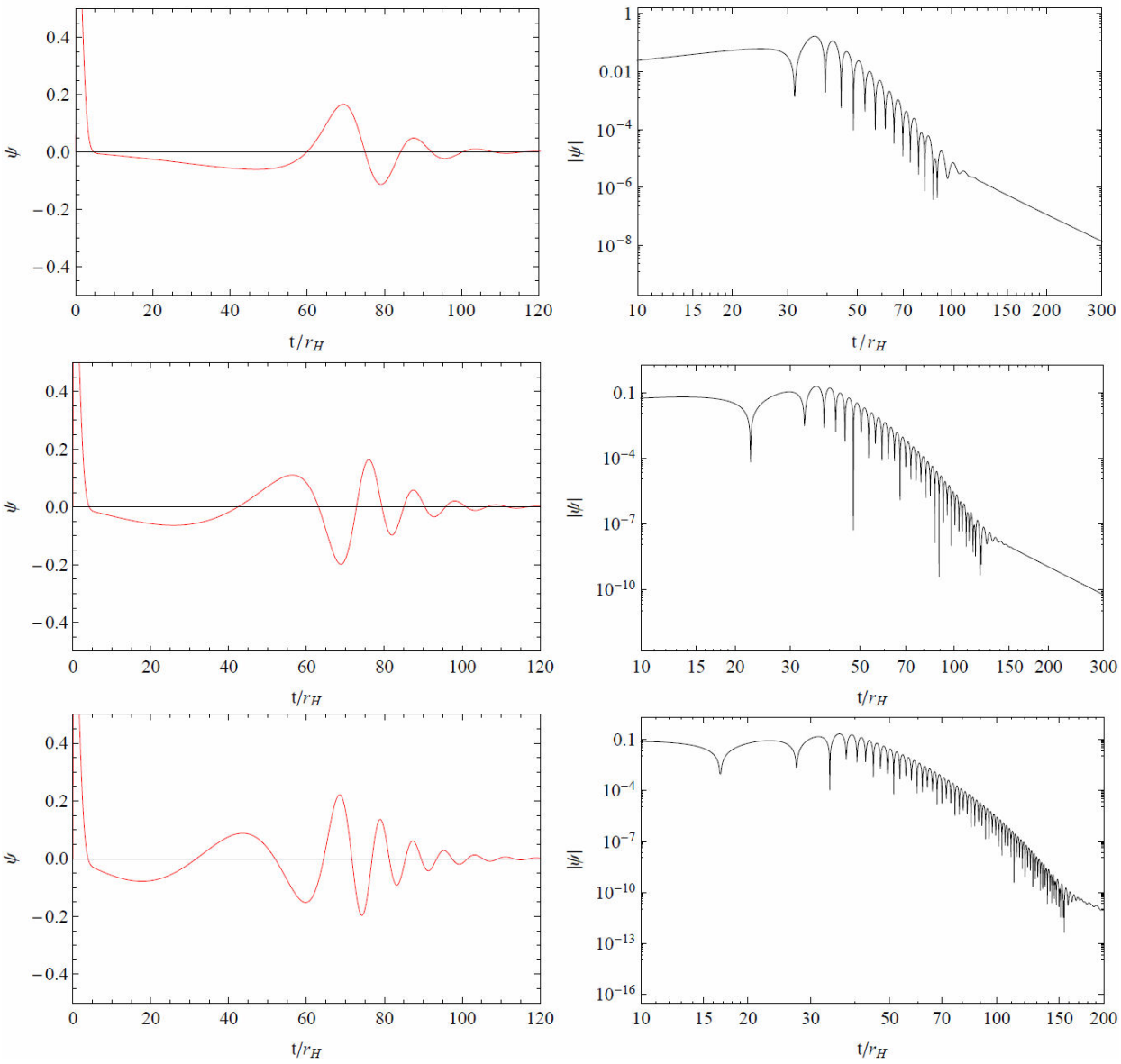

FIGURE 5. Normal (left) and logarithmic (right) plots of the time-domain evolution of massless Dirac perturbations in Bronnikov-Berej's regular black holes with $r_0 = 0.1$. From top to bottom: $\ell = 1, 2, 3$.

of the perturbation and the observation point. This stage is followed by characteristics exponentially damped oscillations, the so called quasinormal vibrations. This phase is known as quasi-normal ringing. Finally, as is usual in asymptotically flat or asymptotically de Sitter space-times, there appear at late times power law tails through which the perturbations die.

It is important to mention that an extensive numerical exploration was performed for several values of the parameters that enter in the regular black hole solutions. Those parameters were chosen such that the considered solution describe non-extreme black holes, with two well defined horizons, and coincides with those used in Ref. 21.

5. Quasi-normal modes

In the following we will assume for the function $\zeta_\ell(t, r)$ the time dependence:

$$\zeta_\ell(t, r) = R_\ell(r) \exp(-i\omega_\ell t), \tag{21}$$

Then, the function $Z_\ell(r)$ satisfy the Schrodinger-like equation:

$$\frac{d^2 R_\ell}{dr_*^2} + \left[\omega^2 - V(r)\right] R_\ell(r) = 0. \tag{22}$$

The quasinormal modes are solutions of the wave equation (12) with boundary conditions requiring pure out-going

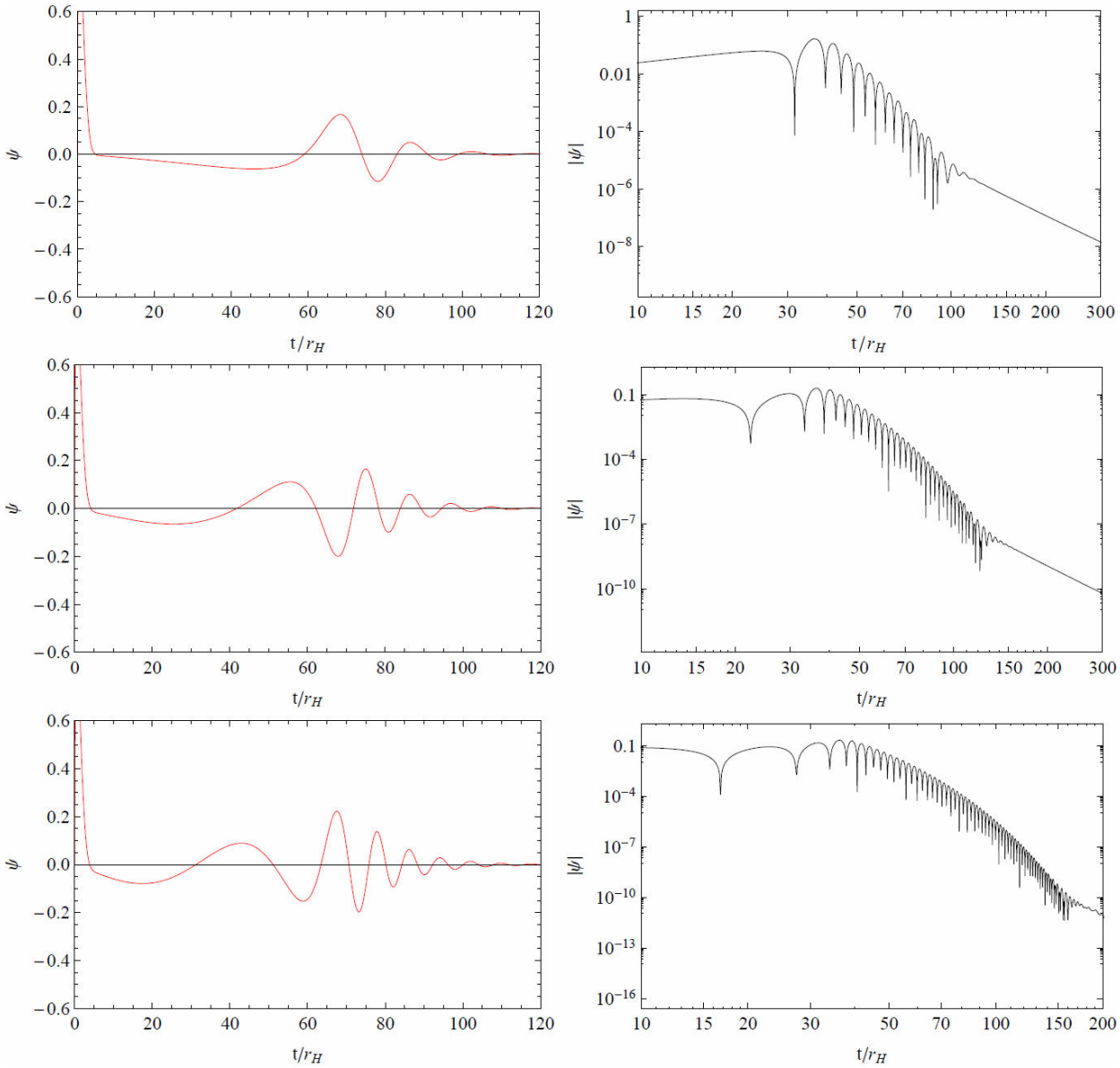

FIGURE 6. Normal (left) and logarithmic (right) plots of the time-domain evolution of massless Dirac perturbations in Dymnikova's regular black holes with $\alpha = 0.1$. From top to bottom: $\ell = 1, 2, 3$.

waves at spatial infinity and pure in-coming waves on the event horizon.

In order to evaluate the quasinormal modes we used two different methods: fitting the numerical data obtained from characteristic and finite difference integration, and a WKB-type semianalytical scheme.

5.1. Fitting the numerical data

The first method uses directly the numerical data obtained previously by finite difference or characteristic integration and fit it. This numerical fitting scheme allow us to obtain very accurate results for the fundamental overtone. For higher overtones is very difficult to be implemented, because

TABLE I. Lowest lying Dirac quasinormal frequencies for the Bardeens's solution, with $m = 1$. The results are obtaining by fitting the appropiate region on the numerical data.

ℓ	n	$\alpha = 0.1$	$\alpha = 0.3$	$\alpha = 0.6$
0	0	$0.1828 - 0.0960i$	$0.1858 - 0.0950i$	$0.1977 - 0.0892i$
1	0	$0.3808 - 0.0963i$	$0.3867 - 0.0953i$	$0.4080 - 0.0897i$
2	0	$0.5738 - 0.0962i$	$0.5818 - 0.0956i$	$0.5860 - 0.0749i$
3	0	$0.7686 - 0.0963i$	$0.7781 - 0.0952i$	$0.8243 - 0.0898i$
4	0	$0.9593 - 0.0961i$	$0.9741 - 0.0952i$	$1.0300 - 0.0897i$
5	0	$1.1529 - 0.0962i$	$1.1690 - 0.0952i$	$1.2442 - 0.0898i$

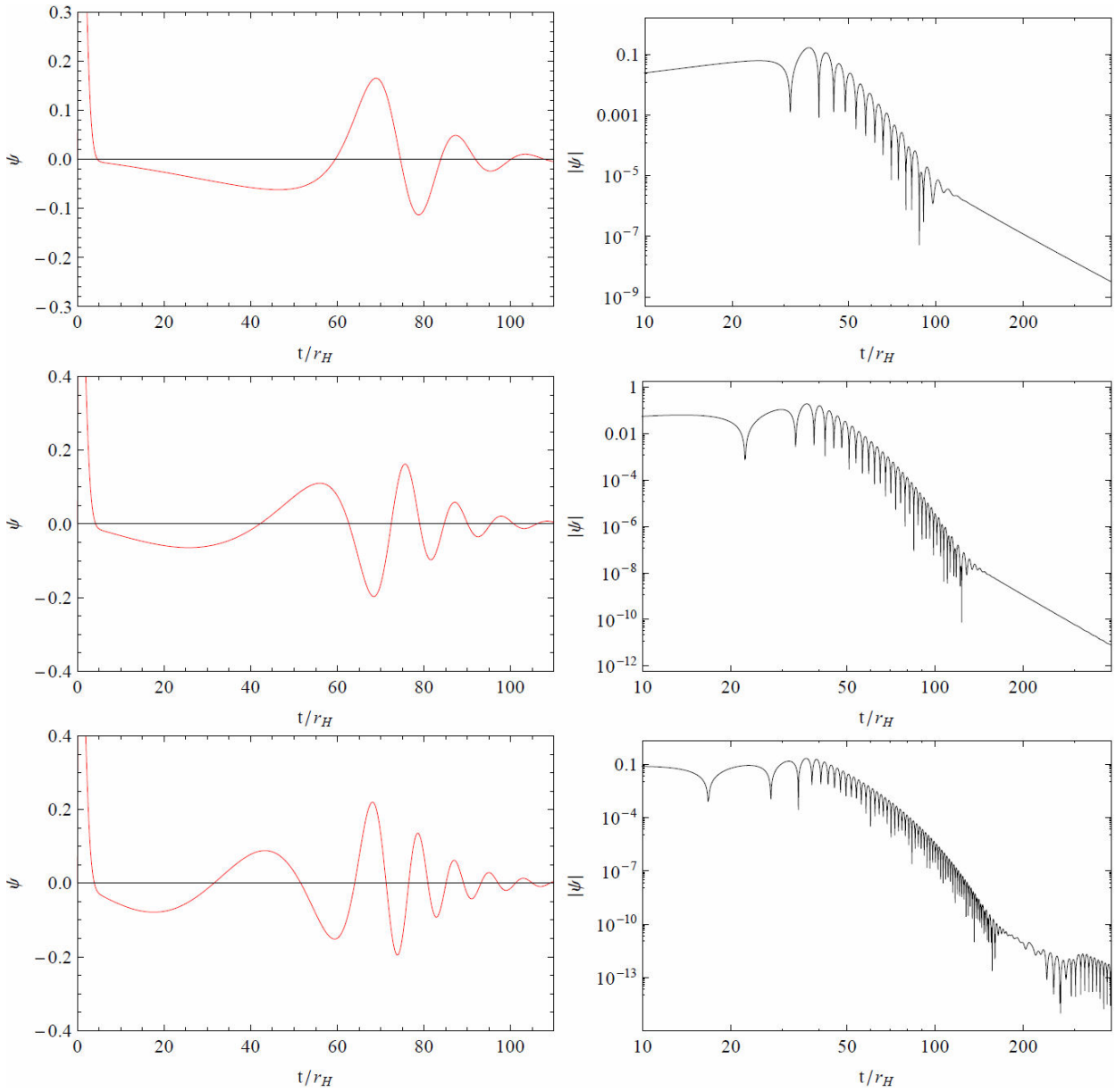

FIGURE 7. Normal (left) and logarithmic (right) plots of the time-domain evolution of massless Dirac perturbations in Ayón-Beato's regular black holes with q=0.1. From top to bottom: $\ell = 1, 2, 3$.

TABLE II. Lowest lying Dirac quasinormal frequencies for the Haywards's solution, with $m = 1$. The results are obtaining by fitting the aproppiate region on the numerical data.

ℓ	n	$\alpha = 0.1$	$\alpha = 0.3$	$\alpha = 0.7$
0	0	$0.1827-0.0961i$	$0.1839-0.0945i$	$0.1893-0.0835i$
1	0	$0.3796-0.0955i$	$0.3800-0.0953i$	$0.3960-0.0850i$
2	0	$0.5756-0.0957i$	$0.57640-0.0949i$	$0.5984-0.0852i$
3	0	$0.7662-0.0962i$	$0.7725-0.0949i$	$0.8004-0.0855i$
4	0	$0.9617-0.0960i$	$0.9666-0.0949i$	$1.0027-0.0855i$
5	0	$1.1564-0.0962i$	$1.1636-0.0949i$	$1.2006-0.0855i$

TABLE III. Lowest lying Dirac quasinormal frequencies for the Bronnikov-Berej's solution, with $m = 1$. The results are obtaining by fitting the aproppiate region on the numerical data.

ℓ	n	$\alpha = 0.1$	$\alpha = 0.3$	$\alpha = 0.4$
0	0	$0.1897-0.0973i$	$0.2086-0.0982i$	$0.2218-0.0973i$
1	0	$0.3935-0.0975i$	$0.4308-0.0983i$	$0.4561-0.0975i$
2	0	$0.5946-0.0973i$	$0.6511-0.0983i$	$0.6879-0.0974i$
3	0	$0.7953-0.0972i$	$0.8666-0.0983i$	$0.9195-0.0974i$
4	0	$0.9973-0.0973i$	$1.0864-0.0983i$	$1.1494-0.0974i$
5	0	$1.1930-0.0973i$	$1.3000-0.0983i$	$1.3809-0.0973i$

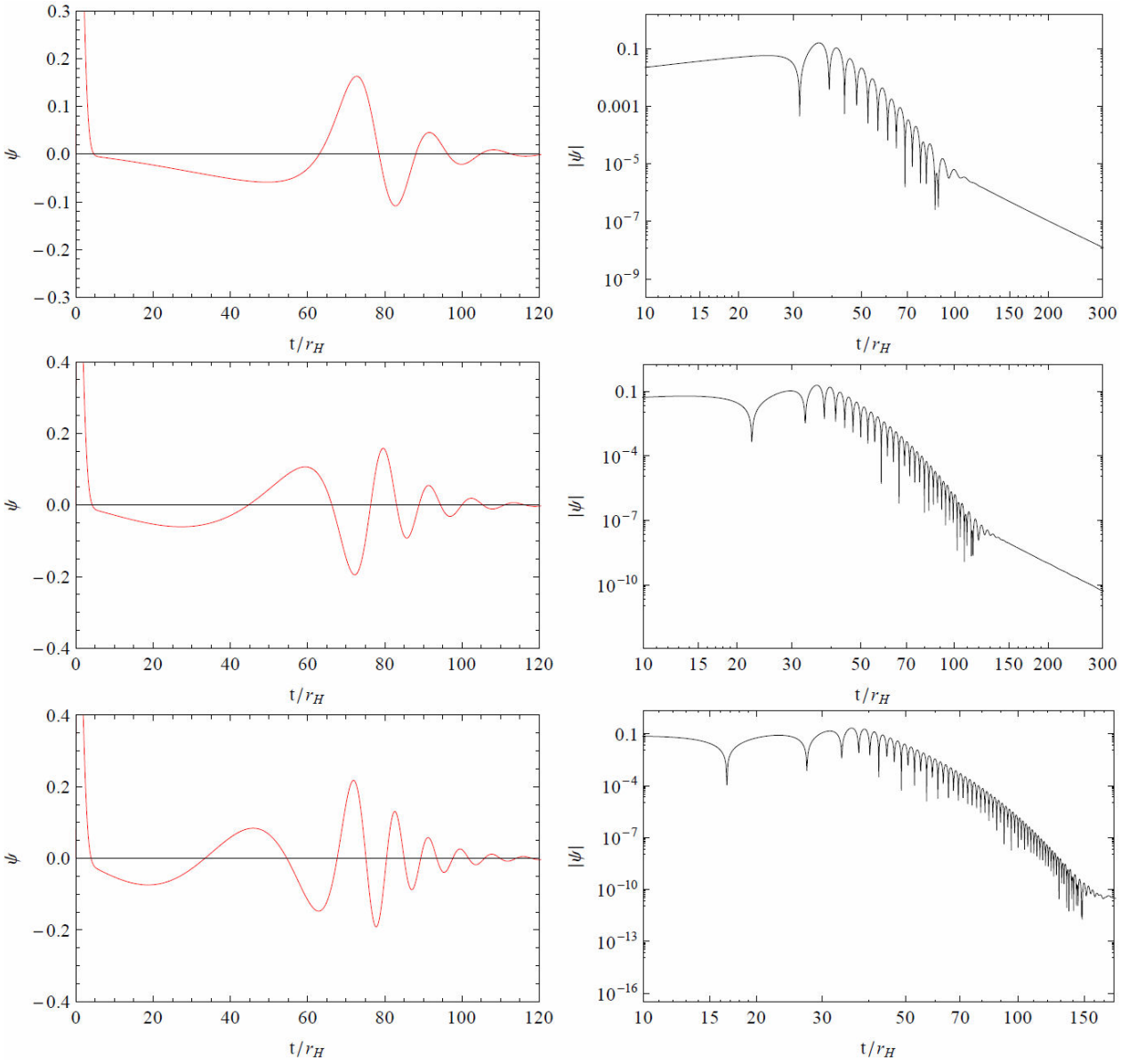

FIGURE 8. Normal (left) and logarithmic (right) plots of the time-domain evolution of massless Dirac perturbations in Bronnikov-Fabris's regular black holes with $b = 0.1$. From top to bottom: $\ell = 1, 2, 3$.

TABLE IV. Lowest lying Dirac quasinormal frequencies for the Dymnikova's solution, with $m = 1$. The results are obtaining by fitting the aproppiate region on the numerical data.

ℓ	n	$r_0 = 0.1$	$r_0 = 0.3$	$r_0 = 0.4$
0	0	$0.1917 - 0.0974i$	$0.2187 - 0.0976i$	$0.2407 - 0.0928i$
1	0	$0.3981 - 0.0978i$	$0.4509 - 0.0979i$	$0.4947 - 0.0933i$
2	0	$0.6013 - 0.0975i$	$0.6793 - 0.0977i$	$0.7450 - 0.0932i$
3	0	$0.8038 - 0.0976i$	$0.9084 - 0.0979i$	$0.9921 - 0.0934i$
4	0	$1.0053 - 0.0975i$	$1.1355 - 0.0978i$	$1.2442 - 0.0934i$
5	0	$1.2083 - 0.0974i$	$1.3659 - 0.0978i$	$1.4901 - 0.0934i$

in the time domain profile, all overtones are present, and it is very difficult to isolate each contribution. For the fundamental overtone, taking into account that the higher ones are more damped and decay very quickly, we can choose a time interval very far from the begining of the quasinormal ringing phase to fit the data. For this reason we only determined the quasinormal frequencies, using this method, for the fundamental overtone.

The numerical results from fitting the numerical data from finite difference integration are presented in Tables I-VI. The results obtained fitting the numerical data from characteristic integration are similar.

TABLE V. Lowest lying Dirac quasinormal frequencies for the Ayón-Beato's solution, with $m = 1$. The results are obtaining by fitting the aproppiate region on the numerical data.

ℓ	n	$q = 0$	$q = 0.3$	$q = 0.6$
0	0	$0.1824-0.0962i$	$0.1891-0.0954i$	$0.2172-0.0846i$
1	0	$0.3800-0.0963i$	$0.3927-0.0956i$	$0.4488-0.0853i$
2	0	$0.5747-0.0964i$	$0.5928-0.0955i$	$0.6768-0.0855i$
3	0	$0.7678-0.0963i$	$0.7920-0.0956i$	$0.9041-0.0856i$
4	0	$0.9593-0.0963i$	$0.9921-0.0956i$	$1.1321-0.0856i$
5	0	$1.1529-0.0963i$	$1.1893-0.0956i$	$1.3610-0.0856i$

TABLE VI. Lowest lying Dirac quasinormal frequencies for the Bronnikov-Fabri's solution, with $m = 1$. The results are obtaining by fitting the aproppiate region on the numerical data.

ℓ	n	$b = 0.1$	$b = 0.5$	$b = 1$
0	0	$0.1824-0.0962i$	$0.1807-0.0968i$	$0.1759-0.0983i$
1	0	$0.3774-0.0965i$	$0.3785-0.0975i$	$0.3660-0.0992i$
2	0	$0.5747-0.0964i$	$0.5695-0.0970i$	$0.5560-0.0993i$
3	0	$0.7678-0.0963i$	$0.7601-0.0969i$	$0.7451-0.0985i$
4	0	$0.9617-0.0963i$	$0.9520-0.0968i$	$0.9286-0.0984i$
5	0	$1.1529-0.0963i$	$1.1424-0.0968i$	$1.1154-0.0984i$

5.2. Sixth order WKB approximation

The second method is a semianalytical one used solve Eq. (22) with the required boundary conditions, based in a WKB-type approximation, that can give accurate values of the lowest, which lives longer, quasinormal frequencies, and was used in several papers to determinate the quasinormal frequencies in a variety of systems [9,11,12,28-32].

The WKB technique was applied to find quasinormal modes for the first time by Shutz and Will [33] and reach up to first order. This approach was extended to the third order beyond the eikonal approximation by Iyer and Will [23] and to the sixth order by Konoplya [34,35]. In our numerical calculation we used this sixth order WKB expansion, which gives a relative error about two orders less than the third WKB order. This expansion allows us to determine the quasinormal frequencies through the formula

$$i\frac{(\omega^2 - V_0)}{\sqrt{-2V_0^{''}}} - \sum_{j=2}^{6}\kappa_j = n + \frac{1}{2}, \qquad (23)$$

where $n = 0, 1, 2, ...$ if $Re(\omega) > 0$ or $n = -1, -2, -3, ..$ if $Re(\omega) < 0$ is the overtone number. In (23) V_0 is the value of the potential at its maximum as a function of the tortoise coordinate, and $V_0^{''}$ represents the second derivative of the potential with respect to the tortoise coordinate at this maximum. The correction terms κ_j depend on the value of the effective potential and its derivatives (up to the 2i-th order) in the peak.

TABLE VII. Quasinormal frequencies for Bardeen's solution with $m = 1$ and various ℓ. WKB results.

ℓ	n	$\alpha = 0.1$	$\alpha = 0.3$	$\alpha = 0.6$
0	0	$0.1830-0.0948i$	$0.1860-0.0936i$	$0.1977-0.0881i$
1	0	$0.3807-0.0963i$	$0.3863-0.0952i$	$0.4090-0.0896i$
2	0	$0.5751-0.0962i$	$0.5833-0.0952i$	$0.6170-0.0898i$
2	1	$0.5581-0.2924i$	$0.5673-0.2891i$	$0.6044-0.2716i$
3	0	$0.7687-0.0962i$	$0.7795-0.0952i$	$0.8243-0.0898i$
3	1	$0.7557-0.2906i$	$0.7673-0.2876i$	$0.8147-0.2707i$
3	2	$0.7313-0.4913i$	$0.7444-0.4857i$	$0.7964-0.4554i$
4	0	$0.9619-0.0961i$	$0.9754-0.0952i$	$1.0314-0.0898i$
4	1	$0.9515-0.2898i$	$0.9656-0.2868i$	$1.0236-0.2702i$
4	2	$0.9313-0.4875i$	$0.9467-0.4822i$	$1.0086-0.4532i$
4	3	$0.9031-0.6916i$	$0.9202-0.6836i$	$0.9872-0.6401i$
5	0	$1.1550-0.0961i$	$1.1712-0.0952i$	$1.2383-0.0898i$
5	1	$1.1463-0.2894i$	$1.1630-0.2864i$	$1.2318-0.2700i$
5	2	$1.1292-0.4854i$	$1.1470-0.4803i$	$1.2191-0.4519i$
5	3	$1.1048-0.6861i$	$1.1240-0.6784i$	$1.2007-0.6368i$
5	4	$1.0743-0.8927i$	$1.0953-0.8821i$	$1.1775-0.8253i$

TABLE VIII. Quasinormal frequencies for Hayward's solution with $m = 1$ and various ℓ. WKB results.

ℓ	n	$\alpha = 0.1$	$\alpha = 0.4$	$\alpha = 0.6$
0	0	$0.1828-0.0947i$	$0.1858-0.0911i$	$0.1893-0.0857i$
1	0	$0.3804-0.0962i$	$0.3849-0.0937i$	$0.3916-0.0890i$
2	0	$0.5745-0.0961i$	$0.5813-0.0937i$	$0.5915-0.0893i$
2	1	$0.5263-0.4980i$	$0.5656-0.2842i$	$0.5765-0.2701i$
3	0	$0.7679-0.0961i$	$0.7770-0.0936i$	$0.7907-0.0893i$
3	1	$0.7549-0.2905i$	$0.7649-0.2828i$	$0.7793-0.2693i$
3	2	$0.7305-0.4910i$	$0.7422-0.4774i$	$0.7573-0.4531i$
4	0	$0.9610-0.0961i$	$0.9723-0.0937i$	$0.9896-0.0893i$
4	1	$0.9505-0.2897i$	$0.9626-0.2822i$	$0.9804-0.2688i$
4	2	$0.9303-0.4873i$	$0.9438-0.4741i$	$0.9624-0.4509i$
4	3	$0.9021-0.6913i$	$0.9174-0.6717i$	$0.9365-0.6370i$
5	0	$1.1539-0.0961i$	$1.1675-0.0937i$	$1.1883-0.0893i$
5	1	$1.1451-0.2892i$	$1.1593-0.2818i$	$1.1806-0.2686i$
5	2	$1.1281-0.4852i$	$1.1435-0.4724i$	$1.1654-0.4497i$
5	3	$1.1035-0.6858i$	$1.1207-0.7000i$	$1.1433-0.6337i$
5	4	$1.0730-0.8923i$	$1.0920-0.8667i$	$1.1150-0.8213i$

Tables VII to XII presents the WKB values obtained for the quasi-normal frequencies with some multipole numbers ℓ for regular black holes with different solution's parameters. As it is observed, the sixth order WKB approach gives results in agreement with those obtained by fitting the numerical integration data.

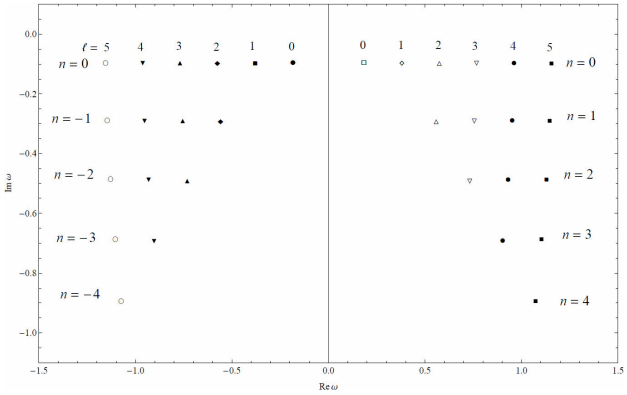

FIGURE 9. Quasinormal modes of Bardeen's regular black hole with $\alpha = 0.1$.

TABLE IX. Quasinormal frequencies for Bronnikov-Berej's solution with $m = 1$ and various ℓ. WKB results.

ℓ	n	$r_0 = 0.1$	$r_0 = 0.3$	$r_0 = 0.4$
0	0	$0.1897-0.0961i$	$0.2084-0.0975i$	$0.2215-0.0967i$
1	0	$0.3940-0.0973i$	$0.4307-0.0983i$	$0.4562-0.0973i$
2	0	$0.5950-0.0973i$	$0.6496-0.0983i$	$0.6877-0.0974i$
2	1	$0.5786-0.2955i$	$0.6356-0.2979i$	$0.6754-0.2946i$
3	0	$0.7951-0.0973i$	$0.8678-0.0983i$	$0.9186-0.0974i$
3	1	$0.7826-0.2939i$	$0.8571-0.2966i$	$0.9091-0.2935i$
3	2	$0.7592-0.4964i$	$0.8369-0.4998i$	$0.8913-0.4937i$
4	0	$0.9950-0.0973i$	$1.0857-0.0983i$	$1.1491-0.0974i$
4	1	$0.9849-0.2931i$	$1.0771-0.2959i$	$1.1415-0.2930i$
4	2	$0.9655-0.4928i$	$1.0604-0.4968i$	$1.1268-0.4913i$
4	3	$0.9384-0.6986i$	$1.0371-0.7027i$	$1.1061-0.6938i$
5	0	$1.1947-0.0972i$	$1.3035-0.0983i$	$1.3795-0.0974i$
5	1	$1.1862-0.2926i$	$1.2963-0.2956i$	$1.3732-0.2927i$
5	2	$1.1698-0.4908i$	$1.2822-0.4951i$	$1.3607-0.4900i$
5	3	$1.1463-0.6933i$	$1.2620-0.6983i$	$1.3428-0.6902i$
5	4	$1.1170-0.9015i$	$1.2367-0.9063i$	$1.3204-0.8943i$

Figure 9 show the quasinormal modes for Bardeen's solution (3). The results obtained for the other regular black hole backgrounds are similar.

As can be easily seen, the behavior of Dirac quasinormal frequencies is analogous to that of the scalar perturbation in regular black holes [21]) as well as Dirac perturbations in other typical black hole backgrounds [7,9-12,36]. The oscillation frequency increases as the multipole number increases for fixed overtone numbers. Concerning the damping rate, increasing ℓ the magnitude of the negative imaginary part of the fundamental overtone ($n = 0$) first increases but then decrease quickly reaching a saturation value for higher multipoles, showing strong similarity with other black hole backgrounds [7,10,36].

For higher overtones the opposite situation arises for the behaviour of the quasinormal frequencies. For a fixed angular number ℓ, the real part of the oscillation frequencies decreases as the overtone number increases, and the magnitude of the imaginary part increases. This is the typical behaviour for back hole backgrounds: higher overtones decay faster than lower ones.

TABLE X. Quasinormal frequencies for Dymnikova's solution with $m = 1$ and various ℓ. WKB results.

ℓ	n	$r_0 = 0.1$	$r_0 = 0.3$	$r_0 = 0.4$
0	0	$0.1919-0.0964i$	$0.2188-0.0972i$	$0.2408-0.0925i$
1	0	$0.3983-0.0976i$	$0.4509-0.0978i$	$0.4943-0.0932i$
2	0	$0.6013-0.0975i$	$0.6797-0.0978i$	$0.7448-0.0933i$
2	1	$0.5852-0.2962i$	$0.6670-0.2961i$	$0.7340-0.2814i$
3	0	$0.8035-0.0975i$	$0.9079-0.0978i$	$0.9946-0.0933i$
3	1	$0.7912-0.2945i$	$0.8982-0.2950i$	$0.9864-0.2809i$
3	2	$0.7681-0.4974i$	$0.8799-0.4964i$	$0.9706-0.4710i$
4	0	$1.0054-0.0975i$	$1.1358-0.0978i$	$1.2441-0.0933i$
4	1	$0.9955-0.2938i$	$1.1280-0.2944i$	$1.2375-0.2806i$
4	2	$0.9764-0.4939i$	$1.1129-0.4938i$	$1.2247-0.4695i$
4	3	$0.9497-0.7000i$	$1.0917-0.6977i$	$1.2061-0.6611i$
5	0	$1.2072-0.0975i$	$1.3636-0.0978i$	$1.4935-0.0933i$
5	1	$1.1989-0.2934i$	$1.3570-0.2941i$	$1.4880-0.2804i$
5	2	$1.1827-0.4919i$	$1.3443-0.4924i$	$1.4772-0.4687i$
5	3	$1.1596-0.6948i$	$1.3259-0.6938i$	$1.4614-0.6588i$
5	4	$1.1307-0.9032i$	$1.3030-0.8994i$	$1.4411-0.8515i$

TABLE XI. Quasinormal frequencies for Ayón-Beato's solution with $m = 1$ and various ℓ. WKB results.

ℓ	n	$q = 0$	$q = 0.3$	$q = 0.6$
0	0	$0.1826-0.0949i$	$0.1893-0.0941i$	$0.2173-0.0836i$
1	0	$0.3801-0.0964i$	$0.3927-0.0956i$	$0.4489-0.0852i$
2	0	$0.5741-0.0963i$	$0.5929-0.0956i$	$0.6771-0.0854i$
2	1	$0.5570-0.2927i$	$0.5773-0.2901i$	$0.6649-0.2576i$
3	0	$0.7674-0.0963i$	$0.7923-0.0955i$	$0.9046-0.0855i$
3	1	$0.7543-0.2910i$	$0.7804-0.2886i$	$0.8953-0.2573i$
3	2	$0.7298-0.4919i$	$0.7581-0.4872i$	$0.8772-0.4313i$
4	0	$0.9603-0.0963i$	$0.9915-0.0955i$	$1.1317-0.0855i$
4	1	$0.9498-0.2901i$	$0.9819-0.2878i$	$1.1243-0.2571i$
4	2	$0.9295-0.4881i$	$0.9634-0.4838i$	$1.1097-0.4301i$
4	3	$0.9011-0.6925i$	$0.9375-0.6856i$	$1.0881-0.6055i$
5	0	$1.1531-0.0962i$	$1.1905-0.0955i$	$1.3588-0.0855i$
5	1	$1.1443-0.2897i$	$1.1824-0.2874i$	$1.3526-0.2570i$
5	2	$1.1271-0.4860i$	$1.1668-0.4819i$	$1.3403-0.4294i$
5	3	$1.1025-0.6869i$	$1.1443-0.6806i$	$1.3221-0.6036i$
5	4	$1.0718-0.8939i$	$1.1163-0.8846i$	$1.2983-0.7800i$

Figures (10)-(11) show the dependence of the quasinormal modes with the different physical parameters that char-

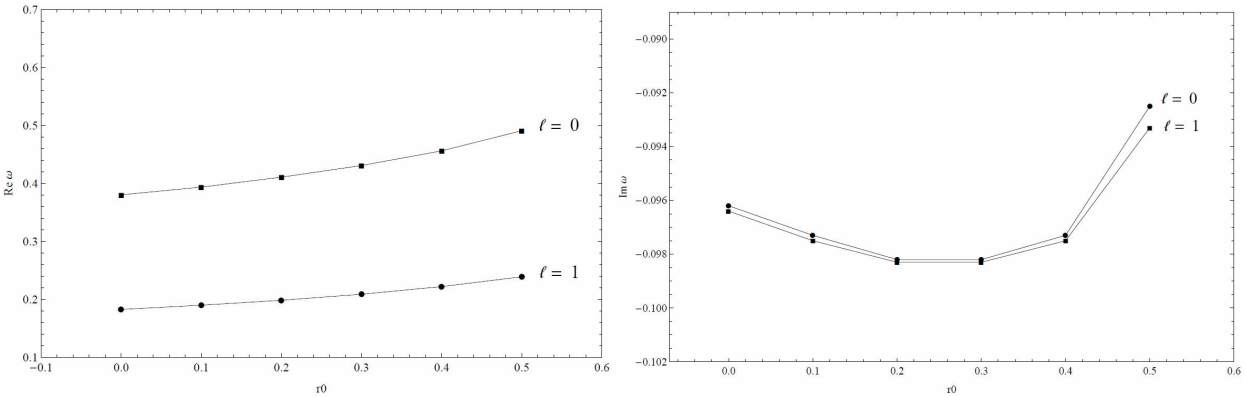

FIGURE 10. Dependance of real (left) and imaginary (right) parts of the first two quasinormal frequencies for Bronnikov-Berej's regular black hole with the parameter r_0.

TABLE XII. Quasinormal frequencies for Bronikov-Fabris's solution with $m = 1$, $c = -(3\pi/2b)$, $\rho = 3$ and various ℓ. WKB results.

ℓ	n	$b = 0.1$	$b = 0.5$	$b = 1$
0	0	$0.1826-0.0950i$	$0.1809-0.0957i$	$0.1756-0.0983i$
1	0	$0.3799-0.0964i$	$0.3768-0.0969i$	$0.3677-0.0985i$
2	0	$0.5739-0.0963i$	$0.5693-0.0968i$	$0.5558-0.0984i$
2	1	$0.5568-0.2928i$	$0.5516-0.2945i$	$0.5362-0.2995i$
3	0	$0.7671-0.0963i$	$0.7610-0.0968i$	$0.7430-0.0983i$
3	1	$0.7540-0.2910i$	$0.7475-0.2927i$	$0.7281-0.2975i$
3	2	$0.7294-0.4920i$	$0.7220-0.4950i$	$0.6999-0.5038i$
4	0	$0.9600-0.0963i$	$0.9524-0.0968i$	$0.9300-0.0983i$
4	1	$0.9494-0.2902i$	$0.9414-0.2918i$	$0.9179-0.2965i$
4	2	$0.9291-0.4882i$	$0.9204-0.4910i$	$0.8946-0.4994i$
4	3	$0.9007-0.6927i$	$0.8910-0.6970i$	$0.8620-0.7098i$
5	0	$1.1527-0.0963i$	$1.1436-0.0968i$	$1.1167-0.0983i$
5	1	$1.1439-0.2898i$	$1.1344-0.2913i$	$1.1066-0.2960i$
5	2	$1.1266-0.4861i$	$1.1166-0.4888i$	$1.0869-0.4969i$
5	3	$1.1020-0.6871i$	$1.0911-0.6911i$	$1.0587-0.7032i$
5	4	$1.0713-0.8941i$	$1.0593-0.8997i$	$1.0235-0.9166i$

acterize some the regular black hole solutions studied in this paper. For all the regular black hole solutions, with the exception of Bronnikov-Fabris's black hole, as the parameter that describes the solution increases, the real part of the quasinormal frequency increases, and the damping rate increases first and then decreases, giving place to a longer ringdown phase. This behavior is similar to that exhibited by a test Dirac field in D-dimensional Reissner-Nordstrom black holes [37,38]. Similar behavior is exhibited by a test scalar field in regular black holes and Reissner-Nordstrom solution [21]), and also gravitino fluctuations in Reissner-Nordstrom backgrounds [39]. However, Bronnikov-Fabris's regular phantom black hole solution shows a different behavior: as the parameter b increases, the actual oscillation frequency decreases, and the damping factor increases. Then, regular phantom black holes becomes more rigid with the increasing of the scalar charge b.

As we can observe from all the above results, all quasinormal frequencies have a definite negative imaginary part, a fact that indicates absence of unstable modes for Dirac perturbations in regular black hole backgrounds. The real question about the stability of such backgrounds is related with the behaviour of proper spacetime fluctuations, a problem that need to be solved in the future. But the fact that Dirac and scalar perturbations in those backgrounds propagates without instabilities, is a good indication for the possible real stability of regular black hole solutions.

An important check of our results can be performed studing the regular black hole solutions in those limits in which they becomes Schwarzschild solution. We determined the quasinormal modes in those limits and obtained the known results. As a representative result, we include in Table XI the frequencies obtained for the Ayón-Beato's solution in the limit $q = 0$.

6. Late-time tails

Another interesting fact to analyse is the relaxation of spinor fluctuations outside the different solutions describing regular black hole backgrounds at very late times [40,41]. To study this late-time behavior, we numerically fit the numerical data obtained from characteristinc integration in the appropriate region of the time domain, to extract the law that describe the relaxation.

In general, all our numerical results indicate that the decay of massless Dirac fields shows a time dependance in the form of a power law, whose exponent changes with the multipole number ℓ, but remain fixed for all values of the physical parameters that describes the different solutions. Also, this power law exponents are the same for all regular black holes, a situations similar to that encountered in the case of four dimensional singular black holes.

In all cases the Dirac perturbations relax at asymptotically late times following a power law proportional to $t^{-(2\ell+3)}$, in strong similarity to the relaxation of fields of different spin in

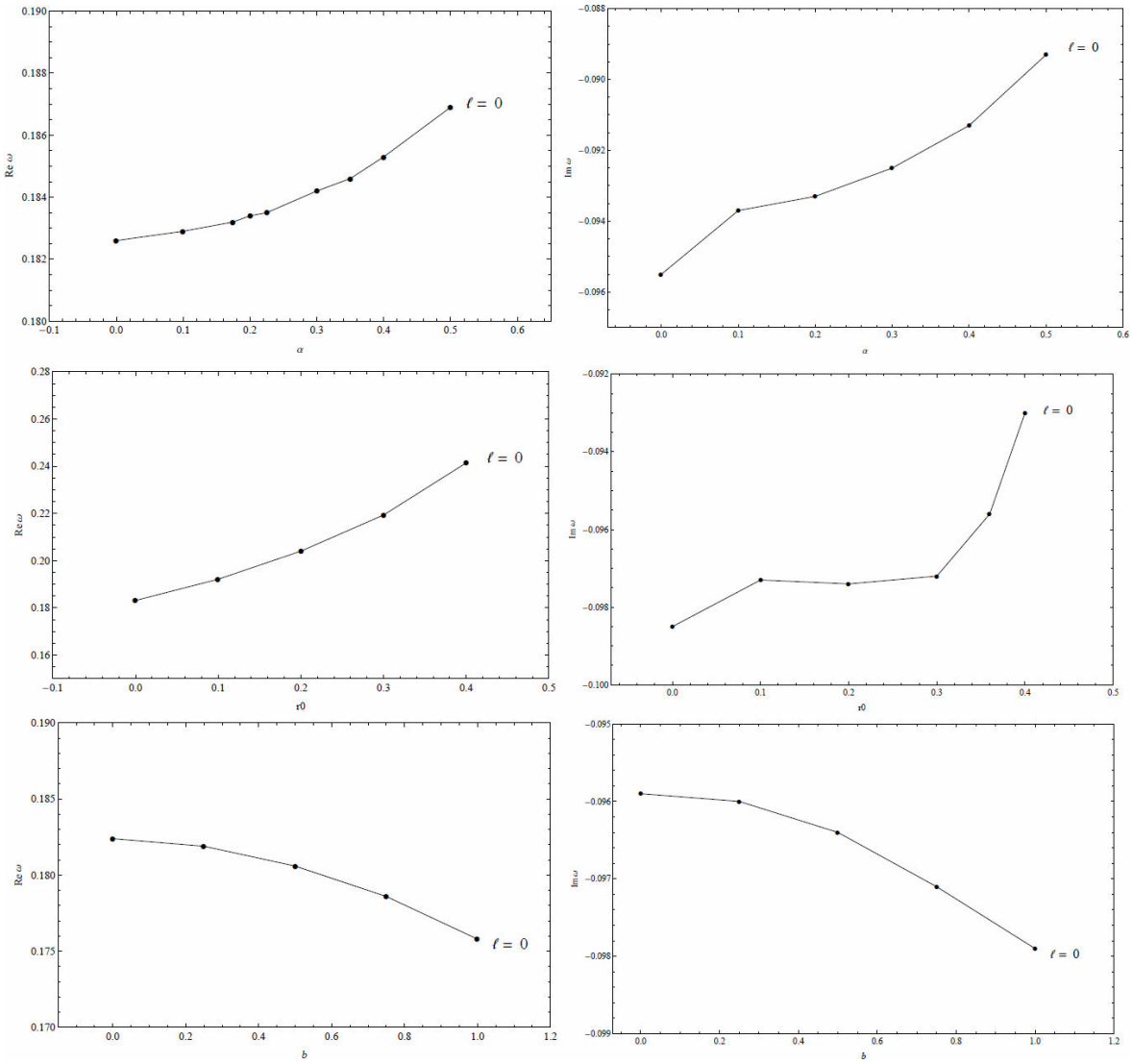

FIGURE 11. Dependance of real (left) and imaginary (right) parts of fundamental quasinormal frequency for regular black holes with the parameters in the solution. From top to bottom we have the results for Hayward's, Dymnikova's and Bronnikov-Fabris's black holes, respectively.

four dimensional Schwarzschild and stringy black hole backgrounds [9,10].

However, we remark at this point that this dependance are only a result consistent with our numerical data. In contrast to the case for boson fields, in which the general form of the effective potential is suitable to expand for large values of the tortoise coordinate [42,43] and then extract the above power law behaviors directly from this asymptotic expansion, a simple analytical argument to support the late time behaviour for fermion test fields do not exist. Then the problem related with the analytical determination of the decay factors for fermion perturbations in regular black holes remains open.

7. Concluding remarks

We have studied the propagation of a massless spinor field outside various regular black hole spacetimes, obtained from theories that couples gravity with source fields, as nonlinear electromagnetic or some phantom matter. We have solved the equation of motion numerically for all cases, using finite difference and characteristic integration methods, and obtain the time domain evolution profile. Fitting the numerical data at the quasinormal ringing stage we determined the quasinormal frequencies. We also compute the quasinormal spectrum using a semi-analytical sixth order WKB approximation. This semianalytical results are in perfect correspondence with the numerical ones.

The quasinormal stage at late times is characterized by damped proper oscillations. We have complex frequencies with negative imaginary part, implying stability of the fermion fluctuations outside the black holes. This picture is the same for all electric and magnetic solutions. The fact that we have found no instabilities for the test field after an extensive explorations with different values of the parameters

that describes the regular black hole solutions considered, is not a direct indication of the stability of the solution itself, although serves as an indication of such stable behaviour. As the charge parameters that characterizes the different solutions increases, the proper frequencies increases and the damping decreases, but this behavior is different for regular phantom black holes, for which an increase in the scalar charge increases the rigidity of the black hole.

We also computed the decay factors for the late time relaxation of spinor perturbations, showing that the fluctuations relaxes in the same way as Dirac waves in other for dimensional non-regular backgrounds.

Some extensions to this work are interesting. First, it would be an important question to determine analytically the late time decay factors, taking into account that for potentials typical of fermion fields do not exist a simple analytical argument to approach this problem, as in the case of boson fields. Also, the study of the evolution of some boson perturbations: electromagnetic and gravitational ones in this space-times would be an interesting subject to be addressed in future reports.

Acknowledgments

This work has been supported by the University of Cienfuegos, Cuba. We would like to express our gratitude to the EJDS service of the ICTP, for giving us the possibility to obtain various references. We also thanks Professor Irina Dymnikova for kindly send a copy of Ref. 18.

1. T. Regge and J.A. Wheeler, *Phys. Rev.* **108** (1957) 1063.
2. K.D. Kokkotas and B. G. Schmidt, *Living Rev. Rel.* **2** (1999) 2.
3. H.-P. Nollert, *Class. Quant. Grav.* **16** (1999) R159.
4. E. Berti, V. Cardoso, and A.O., Starinets, *Class. Quant. Grav.* **26** (2009) 163001.
5. R. A. Konoplya and A. Zhidenko, *Rev. Mod. Phys* **83** (2011) 793.
6. E. Berti, V. Cardoso, J.A. Gonzales and U. Sperhake, *Phys. Rev. D* **75** (2007) 124017.
7. H.T. Cho, A.S. Cornell, J. Doukas and W. Naylor *Phys. Rev. D* **75** (2007) 104005.
8. G. Gibbons and M. Rogatko, *Phys. Rev. D* **77** (2008) 044034.
9. O.P. Fernández Piedra and J. de Oliveira, *Class. Quantum Grav.* **28** (2011) 085023.
10. O.P. Fernández Piedra, *Int. Journal of Mod. Phys. D* **20** (2011) 93.
11. O.P. Fernández Piedra, F. Sosa, José Bernal and Y. Jiménez, *Int. Journal of Mod.Phys. D* **21** (2012) 1250044.
12. O.P. Fernández Piedra, J. Bernal, Y. Jiménez and L. Figueredo, *Int. Journal of Mod.Phys. D* **22** (2013) 1350073.
13. J.M. Bardeen, *Proceedings of GR5* (Tbilisi, USSR) (1968) 174.
14. E. Ayón-Beato and A. García, *Phys. Lett. B* **493** (2000) 149.
15. S.A. Hayward, *Phys. Rev. Lett* **96** (2006) 031103.
16. K.A. Bronnikov, *Phys. Rev. D* **63** (2001) 044005.
17. W. Berej, J. Matyjasek, D. Tryniecki and M. Woronowicz, *Gen. Rel. Grav* **38** (2006) 885.
18. I. Dymnikova *Class. Quant. Grav* **21** (2004) 4417.
19. E. Ayón-Beato and A. García, *Phys. Rev Lett.* **80** (1998) 5056.
20. K.A. Bronnikov and J.C. Fabris, *Phys. Rev Lett.* **96** (2006) 251101.
21. A. Flachi and J.P.S. Lemos, *Phys. Rev. D* **87** (2013) 024034.
22. J. Li, H. Ma and K. Lin, *Phys. Rev. D* **88** (2013) 064001.
23. S. Iyer and C.M. Will, *Phys. Rev*. **D35** (1987) 3621.
24. G. Lopez-Ortega, *Lat. Am. J. Phys. Educ.* **3** (2009) 578.
25. S. Chandrasekar, *The Mathematical theory of Black Holes*, (Clarendon, Oxford, 1983).
26. E. Abdalla, O.P.F. Piedra, F. Sosa and J. de R. Oliveira, *Phys. Rev.* **88** (2013) 064035.
27. C. Gundlach, R. H. Price, J. Pullin, *Phys. Rev.* **49** (1994) 883.
28. R.A. Konoplya and E. Abdalla, *Phys. Rev. D* **71** (2005) 084015.
29. M.I. Liu, H.I. Liu and Y.X. Gui, *Class. Quantum Grav.* **25** (2008) 105001.
30. S. Fernandeo and K. Arnold, *Gen. Rel. Grav.* **36** (2004) 1805.
31. H. Ishihara, M. Kimura, R.A. Konoplya, K. Murata, J. Soda and A. Zhidenko, *Phys. Rev. D* **77** (2008) 084019.
32. E. Abdalla, O.P.F. Piedra and J. de Oliveira, C. Molina, *Phys. Rev. D* **81** (2010) 064001.
33. B. Schutz and C.M. Will, *Astrophys. J. Lett. L* **33** (1985) 291.
34. R.A. Konoplya, *Phys. Rev. D* **68** (2003) 024018.
35. R.A. Konoplya, *J. Phys. Stud*. **8** (2004) 93.
36. J. Jing, *Phys. Rev. D* **71** (2005) 124006.
37. J. Jing, *JHEP* **0512** (2005) 005.
38. S. Chakrabarty, *Eur. Phys. J. C.* **61** (2009) 477.
39. F. Shu and Y. Shen, *Phys. Lett. B* **614** (2005) 195.
40. R.H. Price, *Phys. Rev. D* **5** (1972) 2419.
41. R.H. Price and L.M. Burko, *Phys. Rev. D* **70** (2004) 084039.
42. E.S.C. Ching, P.T. Leung, W.M. Suen and K. Young, *Phys. Rev. Lett.* **74** (1995) 2414.
43. E.S.C. Ching, P.T. Leung, W.M. Suen and K. Young, *Phys. Rev. D* **52** (1995) 2118.